

Preparation and Crystal Structure Determination of Sulphur Dioxide Solvate Crystals with Cetyl- and Dodecyltrimethylammonium Bromide

Denitsa Shopova, Robert Dinnebier, and Martin Jansen

Max Planck Institute for Solid State Research, Heisenbergstraße 1, 70569 Stuttgart, Germany

Reprint requests to Prof. M. Jansen. E-mail: M.Jansen@fkf.mpg.de

Z. Naturforsch. **2008**, *63b*, 1087–1092; received May 6, 2008

Cetyltrimethylammonium bromide (CTAB) and dodecyltrimethylammonium bromide (DTAB) form with sulphur dioxide crystalline solvates which have been characterised by Raman spectroscopy and X-ray powder diffraction (XRPD) at room temperature. In both crystal structures, the fully extended CTAB and DTAB cations are oriented along the *a* axes, forming infinite parallel stacks along the *b* axes. Neighbouring stacks form sheets with the bromide anions and the sulphur dioxide molecules acting as chelating agents. Consecutive sheets are flipped and shifted, thus building the three-dimensional crystal structure in a brick-like manner.

Key words: Surfactant, Sulphur Dioxide Adducts, Crystal Structure, CTAB, DTAB

Introduction

The main purpose for the use of ionic surfactants such as quaternary ammonium salts, *e. g.* cetyltrimethylammonium bromide (CTAB), dodecyltrimethylammonium bromide (DTAB) or cetyltrimethylammonium chloride (CTAC), is to form spherical micelles in water, formamide, glycerol, or ammonia at concentrations above a critical micelle concentration [1, 2]. The compounds contain a long hydrocarbon chain and a lyophilic head, which induce the formation of micelle structures. In addition, ionic surfactants can form complexes with different aromatic hydrocarbons [3], phenol derivatives [4–6], guaiacol, 2-methylindole, skatole [7], and perchlorates [8] in aqueous solutions.

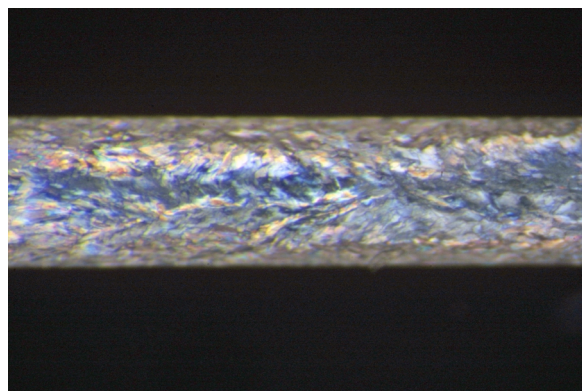


Fig. 1. Magnified image (40 \times) of fibrous crystallites of $C_{16}H_{33}N(CH_3)_3 \cdot Br \cdot SO_2$ (**2**) under crossed polarisers crystallised at the inner wall of a quartz capillary.

In this paper, we report two new crystal structures of molecular complexes containing the common surfactants DTAB and CTAB and sulphur dioxide as the only solvate molecule: $C_nH_{2n+1}N(CH_3)_3 \cdot Br \cdot SO_2$ with $n = 12$ (**1**), and $n = 16$ (**2**). Due to the fact that single crystals of sufficient size and quality for single crystal diffraction could not be obtained, the crystal structures of **1** and **2** were determined from high-resolution powder diffraction on *in situ* synthesised microcrystalline samples. To verify the inclusion of sulphur dioxide in the crystalline material, the new compounds were additionally characterised by Raman spectroscopy.

Experimental Section

Synthesis

CTAB (Roth, > 98 %) was dried in vacuum for several hours at $T = 100$ °C. About 5 mg of the substance was filled under argon into a quartz capillary ($d = 0.5$ mm) using a Schlenk technique. After evacuation of the complete system, the capillary was cooled with liquid nitrogen, and sulphur dioxide (Gerling Holz & Co, 3.8, dried over calcium hydride) was condensed onto it. CTAB dissolved easily in SO_2 turning the solution yellow. After complete solvation, part of SO_2 was re-condensed, and the residue (~ 0.002 g) was frozen. Small fibers of the obtained molecular complex crystallised at the inner wall of the capillary (Fig. 1). Finally, the capillary was sealed under vacuum. The weights of the materials were determined with an accuracy of ± 0.1 mg. The same procedure was used for the synthesis of the compound DTAB- SO_2 .

Raman spectra

Raman spectra were measured at r.t. in the range from 100 to 3500 cm^{-1} (Jobin-Yvon, LabRam operating at the wavelength of 632.8 nm from a He-Ne laser). The spectra were taken directly on the quartz capillary.

X-Ray powder diffraction (XRPD)

High-resolution powder diffraction patterns of **1** and **2** were collected at r.t. on a laboratory powder diffractometer (D-8, Bruker, $\text{CuK}\alpha_1$ radiation from a primary Ge(111) Johansson-type monochromator). A Vantag-1 position-sensitive detector (PSD) with an opening angle of 6° in Debye-Scherrer geometry with the samples sealed in quartz capillaries of 0.5 mm diameter (Hilgenberg) was used. Data were taken in steps of $2\theta = 0.009^\circ$ in the range $2\theta = 2.0\text{--}60.0^\circ$ over a period of 21 h (Fig. 2). The samples were spun during measurement for better particle statistics. For indexing

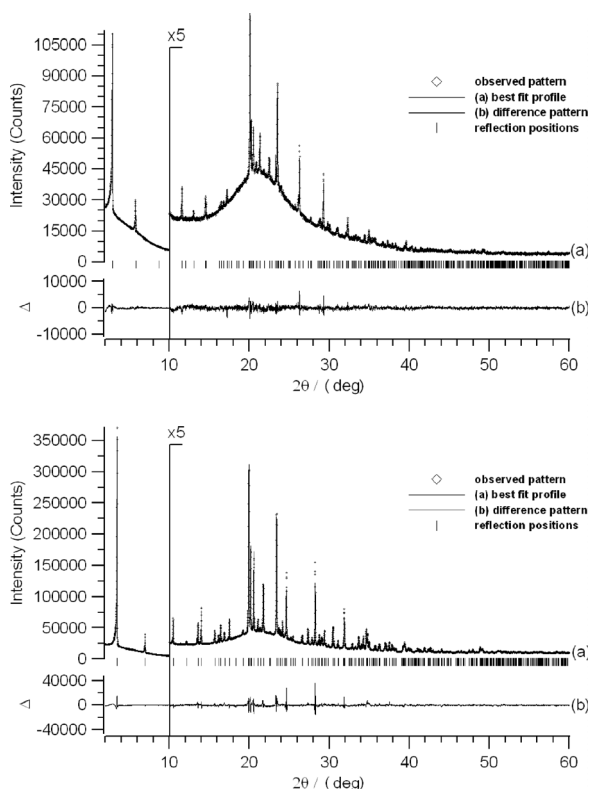


Fig. 2. Scattered X-ray intensities for **2** (top) and **1** (bottom), $T = 295$ K, as a function of the diffraction angle 2θ . Shown are the observed pattern (diamonds), the best Rietveld-fit profile in $Pna2_1$ (line a), the difference curve between the observed and calculated profile (line b), and the reflection markers (vertical bars). The wavelength was $\lambda = 1.54059$ Å. The higher angle part starting at $2\theta = 10^\circ$ is enlarged by a factor of 5.

Table 1. Crystallographic data for $\text{C}_{12}\text{H}_{25}\text{N}(\text{CH}_3)_3 \cdot \text{Br} \cdot \text{SO}_2$ (**1**) and $\text{C}_{16}\text{H}_{33}\text{N}(\text{CH}_3)_3 \cdot \text{Br} \cdot \text{SO}_2$ (**2**).

	1	2
Formula	$\text{C}_{12}\text{H}_{25}\text{N}(\text{CH}_3)_3 \cdot \text{Br} \cdot \text{SO}_2$	$\text{C}_{16}\text{H}_{33}\text{N}(\text{CH}_3)_3 \cdot \text{Br} \cdot \text{SO}_2$
M_r	372.41	428.52
Crystal system	orthorhombic	orthorhombic
Space group	$Pna2_1$ (no. 33)	$Pna2_1$ (no.33)
a , Å	50.4791(6)	60.9215(8)
b , Å	5.5130(1)	5.4569(1)
c , Å	7.5845(1)	7.5546(1)
V , Å ³	2110.70(5)	2511.44(7)
Z	4	4
D_{calcd} , g cm^{-3}	1.172	1.133
Radiation; λ , Å	$\text{CuK}\alpha_1$; 1.54059	$\text{CuK}\alpha_1$; 1.54059
Starting angle 2θ , deg	2.0	2.0
Final angle 2θ , deg	60.0	60.0
Step width 2θ , deg	0.009	0.009
Scan time, h	21	21
No. of variables	49	48
$R\text{-exp}$, % ^a	1.23	1.31
$R\text{-p}$, % ^a	3.36	1.59
$R\text{-wp}$, % ^a	4.66	2.07
$R\text{-}F^2$, % ^a	1.34	0.49
Reduced χ^2	3.78	1.58

^a $R\text{-exp}$, $R\text{-p}$, $R\text{-wp}$, and $R\text{-}F^2$ as defined in the program TOPAS [9].

of the powder patterns of **1** and **2**, the program TOPAS-I [9] was used. Indexing was performed by iterative use of singular value decomposition (LSI) [10], leading to primitive orthorhombic unit cells with the lattice parameters given in Table 1. For both compounds, the most probable space group could be determined as $Pnma$ or $Pna2_1$ from the observed extinction rules. The number of formula units per unit cell could be determined to be $Z = 4$ from packing considerations. Cell volumes of 2111 Å³ for **1** and 2512 Å³ for **2** in the space group $Pna2_1$ suggested only one formula unit of these complexes in the asymmetric unit. The crystal structures of **1**, and **2** were solved by the global optimisation method of simulated annealing in real space using the DASH structure solution package [11]. The measured powder patterns were subjected to Pawley refinements [12] in space groups $P2_12_12_1$ and $Pna2_1$ in order to extract correlated integrated intensities from the patterns. Good fits to the data were obtained. For the description of the components, the dodecyl- and hexadecyltrimethylammonium cations and the sulphur dioxide molecules were constructed in ISISTM/Draw 2.4 (MDL Information Systems, Inc.) using standard bond lengths and angles from compounds containing identical molecules [13–15]. For the definition of the connectivity between the atoms within the molecule, the Z-matrix notation was used, which allows for the description of the entire molecule and its intramolecular degrees of freedom by employing interatomic distances, angles and dihedral angles. All intramolecular angles and distances were kept fixed at standard values. For solving the crystal structures of **1** and **2**, 12 external degrees

Table 2. Atomic coordinates and isotropic displacement parameters for non-hydrogen atoms in **1** and **2**.

	Atom	x	y	z	B _{iso}
1	Br1	0.468	0.124	0.750	3.67
	S1	0.911	0.415	0.718	10.01
	O2	0.906	0.421	0.904	10.01
	O3	0.909	0.656	0.649	10.01
	N17	0.542	0.510	0.751	6.37
	C1	0.839	0.576	0.679	6.37
	C2	0.815	0.723	0.714	6.37
	C3	0.790	0.559	0.688	6.37
	C4	0.765	0.706	0.724	6.37
	C5	0.740	0.542	0.696	6.37
	C6	0.715	0.689	0.735	6.37
	C7	0.691	0.527	0.708	6.37
	C10	0.665	0.675	0.747	6.37
	C13	0.641	0.515	0.720	6.37
	C14	0.615	0.664	0.763	6.37
	C15	0.591	0.506	0.734	6.37
	C16	0.566	0.655	0.779	6.37
	C18	0.539	0.337	0.896	6.37
	C19	0.544	0.376	0.583	6.37
	C20	0.518	0.671	0.746	6.37
2	Br1	0.474	0.118	0.750	4.97
	S1	0.926	0.501	0.721	9.92
	O2	0.921	0.251	0.687	9.92
	O3	0.921	0.558	0.902	9.92
	N17	0.537	0.505	0.737	10.01
	C1	0.866	0.553	0.797	10.01
	C2	0.845	0.706	0.811	10.01
	C3	0.825	0.537	0.785	10.01
	C4	0.804	0.690	0.799	10.01
	C5	0.784	0.522	0.774	10.01
	C6	0.763	0.675	0.790	10.01
	C7	0.743	0.508	0.764	10.01
	C8	0.722	0.662	0.782	10.01
	C9	0.701	0.498	0.756	10.01
	C10	0.680	0.653	0.777	10.01
	C11	0.660	0.491	0.749	10.01
	C12	0.639	0.648	0.772	10.01
	C13	0.619	0.489	0.743	10.01
	C14	0.598	0.647	0.769	10.01
	C15	0.577	0.490	0.738	10.01
C16	0.557	0.649	0.767	10.01	
C18	0.533	0.339	0.887	10.01	
C19	0.539	0.359	0.574	10.01	
C20	0.518	0.671	0.720	10.01	

of freedom were subjected to global optimisation [16]: three translations and three rotations for the do/hexadecyltrimethylammonium cations and sulphur dioxide molecules each, and three translations for the bromide anions. In addition, the CH₂-N(CH₃)₃ torsion angle of the cations was included in the structure determination process as an internal degree of freedom.

In the beginning, no more torsion angles were introduced for the global optimisation since from literature it is well known that DTAB and CTAB cations are fully extended in

Table 3. Intra- and intermolecular distances (Å) and angles (deg) for the non-hydrogen atoms of **1** and **2**.

	1	2
Distances fixed		
Br–C min	3.789(4) ^a	3.771(6) ^a
	3.919(3) ^b	3.954(4) ^b
Br–O min	3.368(6)	3.350(1)
Br–H min	2.847(1) ^a	2.942(3) ^a
	2.977(5) ^b	3.002(9) ^b
C–C	1.538(2)–1.599(4)	1.546(9)–1.599(4)
N–C	1.469(7)–1.479(9)	
Angles fixed		
–CH ₂ –N(CH ₃) ₃ torsion angle	15.6(7)	14.1(9)
N–C–C	110.8(4)	
C–N–C	109.0(7)–110.8(4)	
C(16)–C(15)–C(14)	109.1(4)–109.7(2)	

^a Distance to atom of neighbouring layer; ^b distance to atom within the layer.

most structures with only very few torsion angles within the carbon chain deviating by more than 10° from 180°. The structure giving the best fit to the data in space group *Pna2*₁ was validated by Rietveld refinement using the program TOPAS 3.0 [9]. The peak profiles and precise lattice parameters were first determined by a LeBail fit [17] using the fundamental parameter (FP) approach of TOPAS [18]. Due to the fact that the geometry of the Vântag-1 PSD is not fully characterised by FP's, fine tuning of the available parameters was performed by using refined values of the FP's from a precise measurement of the NIST line profile standard SRM 660a (LaB₆) in a 0.1 mm capillary over the full 2θ range of the diffractometer. Since the origin in space group *Pna2*₁ is floating in *z* direction, the *z* coordinate of the bromine atom was fixed to 3/4.

Interestingly, the intensities of all *h00* reflections increased with increasing diffraction order relative to the values calculated from the structural model. This puzzling effect for a capillary setup can be understood from the microscopic and the macroscopic picture of the compounds under investigation. The extremely anisotropic crystalline lattice, with the elongated molecules being almost perfectly oriented along the *a* direction, is macroscopically visible in the fibrous crystallites. The fibers of the plastic crystallites have grown at the inner walls along the quartz capillary, preferably pointing to the centre of the capillary. Thus, the *h00* intensities are affected by a combination of preferred orientation (even in the capillary setup) and absorption effects, since the reflections at higher angles penetrate less deeply into the capillary. Since almost exclusively *h00* reflections are affected with increasing relative intensity at higher order, the effect could effectively be modeled by scaling the *h00* peaks with a user defined function of type $a^b + b$. This empirically derived two-parameter function could be easily implemented into the TOPAS input file and proved to be more efficient than the 6

parameters of the symmetrised spherical harmonics correction of 4th order.

The refinement of the torsion angles within the carbon chain of the DTAB and CTAB cations did neither lead to meaningful changes in the crystal structure, nor to an improvement of the agreement factors, but led to high correlations in between and was therefore discarded. Three isotropic displacement parameters for the do/hexadecyltrimethylammonium cation, the bromine anion and the SO₂ molecule were refined. The final agreement factors are listed in Table 1. The atomic coordinates are given in Table 2, and a selection of intra- and inter-molecular distances and angles is given in Table 3.

CCDC 661744 and CSD 661743 contain the supplementary crystallographic data for this paper. These data can be obtained free of charge from The Cambridge Crystallographic Data Centre *via* www.ccdc.cam.ac.uk/data_request/cif.

Results and Discussion

Raman spectra of $C_nH_{2n+1}N(CH_3)_3 \cdot Br \cdot SO_2$ ($n = 12, 16$)

Fig. 3 (top) shows the Raman spectrum of $C_{16}H_{33}N(CH_3)_3 \cdot Br \cdot SO_2$ (**2**) as measured at r. t., exhibiting all Raman active bands of the components [19–21]. The spectrum can be described as a superposition of the spectra of CTAB and SO₂. The intensities of the observed bands of CTAB in the new compound are different, but all the modes exist. The most intensive band at 1130 cm⁻¹ corresponds to ν_s of sulphur dioxide [19, 22]. The ν_{as} band is also present at 1326 cm⁻¹ with weak intensity. The Raman spectrum of **1** shows the same superposition of the lines of DTAB and SO₂.

Crystal structure determination

Despite of a high overall displacement parameter, which is in agreement with similar structures [13], all molecules in the crystal structures of **1** and **2** appear to be ordered in well defined positions. This observation is corroborated by the fact that only little strain broadening was observed in the powder patterns of **1** and **2**.

The CTAB and DTAB cations are fully extended in direction of the *a* axes. The longest principal axes of the cations form angles between 1.74° (CTAB) and 3.6° (DTAB) with the *ac* plane. These values are different from those reported for the unsolvated surfactant compounds: 68° (DTAB) [6, 14] and 65° (CTAB) [13]. The lyophilic head is formed by the ammonium groups

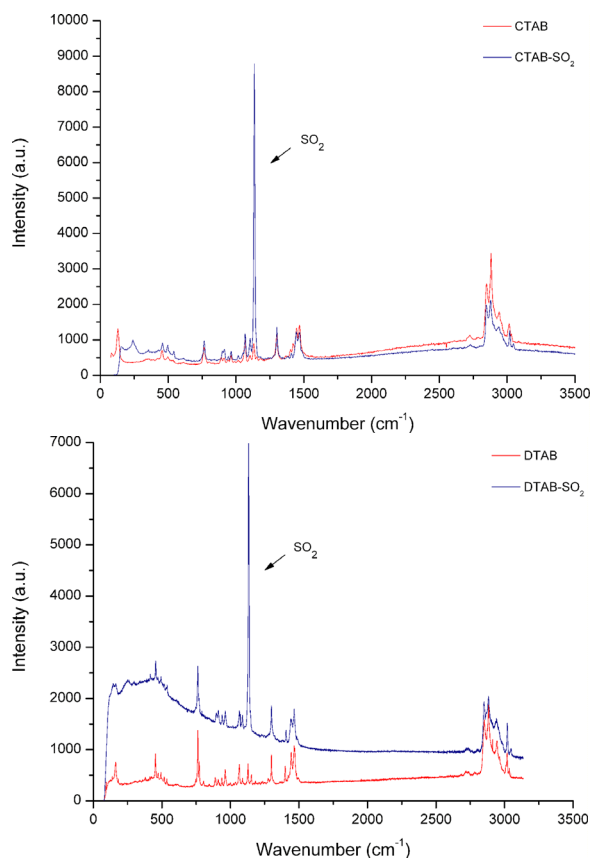


Fig. 3. Raman spectra of $C_nH_{2n+1}N(CH_3)_3 \cdot Br \cdot SO_2$ (blue) (top: **2**; bottom: **1**) and CTAB or DTAB (red) measured at r. t., $\lambda = 632.8$ nm, clearly showing the characteristic SO₂ mode at $\nu_s = 1130$ cm⁻¹ (colour online).

and the bromine anions, while the lyophobic tail is formed by the hydrocarbon chains. The CTAB and DTAB cations form infinite stacks along the *b* axis (Fig. 4). The hydrocarbon chains of neighbouring stacks along the *a* axis are packed “head to tail” with a molecule of SO₂ in between the stacks, thus forming a layer-type structure. Neighbouring stacks are shifted by 1/2 *b* along the *b* axis. Consecutive layers along the *c* axes are flipped and shifted by 1/2 *a* along the *a* axis.

$Br \cdot SO_2 \cdot C_nH_{2n+1}N(CH_3)_3$ with $n = 12$ (**1**), and $n = 16$ (**2**) are forming closely related crystal structures in space group $Pna2_1$ ($Z = 4$), with lattice parameters of $a = 50.4791(6)$, $b = 5.5130(1)$, $c = 7.5845(1)$ Å, and $V = 2110.70(5)$ Å³ for **1**, and $a = 60.9215(8)$, $b = 5.4569(1)$, $c = 7.5546(1)$ Å, and $V = 2511.44(7)$ Å³ for **2**. Despite the different crystal systems and the different orientations of the molecules in the unit cells,

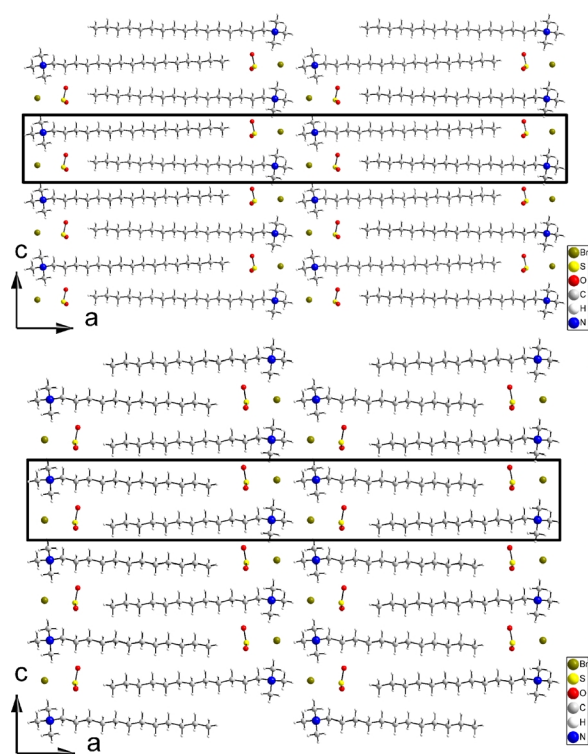


Fig. 4. Packing of **2** (top) and **1** (bottom) in the crystal at $T = 295$ K.

the general packing in **1** and **2** is very similar to the crystal structures of solvent free DTAB and CTAB [6, 13, 14]. The main difference is the extended dis-

tance between the molecules within a layer, due to the presence of sulphur dioxide as solvate. Therefore, the cell axes in direction of the carbon chains are considerably larger, while the other cell dimensions are in good agreement with those of the solvent free counterparts [6, 13, 14].

The electrostatic interactions between the ammonium groups and the bromide anions and the van der Waals contacts between methyl and methylene groups stabilise the aggregate. Caused by the shifts between the layers, the arrangement of the bromide ions in the crystal structures is in a zig-zag manner. The distances between the bromide anion and the methyl groups of the $N(\text{CH}_3)_3$ group within a layer lie in the range 3.919–4.255 Å for **1** and 3.954–4.386 Å for **2**. On the other hand, the distance between the same bromide ion and the methyl group from a neighbouring layer is only 3.789 (**1**) or 3.835 Å (**2**). We regard this as the main reason for the stability of this bi-layer structure. The distances between the nitrogen atom and the bromide anion are 4.322 (**1**) and 4.376 Å (**2**) in the same layer, and 4.287 or 4.328 Å (**1**), 4.433 or 4.259 Å (**2**) in adjacent layers. It is interesting to note that the crystal structures of the soft compounds reported here are stable and stay fully ordered even at r. t.

Acknowledgement

Financial support by the Bundesministerium für Bildung und Forschung (BMBF), and the Fonds der Chemischen Industrie (FCI) is gratefully acknowledged.

- [1] X. Auvray, C. Petipas, R. Anthore, I. Rico, A. Lattes, *J. Phys. Chem.* **1989**, *93*, 7458–7464.
- [2] S. Bzik, M. Jansen, *Chem. Eur. J.* **2003**, *9*, 614–620.
- [3] K. Sawada, T. Kitamura, Y. Ohashi, N. Iimura, H. Hirata, *Bull. Chem. Soc. Jpn.* **1998**, *71*, 2109–2118.
- [4] F. Toda, K. Tanaka, T. Okada, S. Bourne, L. Nassimbeni, *Supramol. Chem.* **1994**, *3*, 291–298.
- [5] N. Yamada, M. Iijima, K. Vongbupnimit, K. Noguchi, K. Okuyama, *Angew. Chem.* **1999**, *111*, 969–972; *Angew. Chem. Int. Ed.* **1999**, *38*, 916–918.
- [6] S. Kamitori, Y. Sumimoto, K. Vongbupnimit, K. Noguchi, K. Okuyama, *Mol. Cryst. Liq. Cryst.* **1997**, *300*, 31–43.
- [7] N. Iimura, Y. Ohashi, H. Hirata, *Bull. Chem. Soc. Jpn.* **2000**, *73*, 1097–1103.
- [8] M. Udupa, *Thermochim. Acta* **1982**, *52*, 363.
- [9] A. A. Coelho, TOPAS, Bruker AXS GmbH, Karlsruhe (Germany) **2006**.
- [10] A. A. Coelho, *J. Appl. Crystallogr.* **2003**, *36*, 86–95.
- [11] W. I. F. David, K. Shankland, J. van de Streek, E. Pidcock, W. D. S. Motherwell, J. C. Cole, DASH, A Program for Crystal Structure Determination from Powder Diffraction Data, Cambridge Crystallographic Data Centre, Cambridge (U. K.) **2006**. See also: *J. Appl. Cryst.* **2006**, *39*, 910–915.
- [12] G. S. Pawley, *J. Appl. Crystallogr.* **1981**, *14*, 357–361.
- [13] R. Campanelli, L. Scaramuzza, *Acta Crystallogr.* **1986**, *C42*, 1380–1383.
- [14] K. Szulzewsky, B. Schulz, D. Vollhardt, *Crystal Res. & Technol.* **1983**, *18*, 1003–1008.
- [15] B. Post, R. Schwartz, I. Frankuchen, *Acta Crystallogr.* **1952**, *5*, 372–374.
- [16] W. I. F. David, K. Shankland, N. Shankland, *Chem. Commun.* **1998**, *8*, 931–932.
- [17] A. Le Bail, H. Duroy, J. Fourquet, *Mater. Res. Bull.* **1988**, *23*, 447–452.
- [18] R. W. Cheary, A. A. Coelho, J. P. Cline, *J. Res. Natl. Inst. Stand. Technol.* **2005**, *109*, 1–25.

- [19] M. Kamoun, *J. Raman Spectr.* **1979**, 8, 225–226.
- [20] K. Kalyanasundaram, J. Thomas, *J. Phys. Chem.* **1976**, 80, 1462–1473.
- [21] R. Foucault, R. Birke, J. Lombardi, *Langmuir* **2003**, 19, 8818–8827.
- [22] A. Kornath, O. Blecher, *Z. Anorg. Allg. Chem.* **2002**, 628, 570–574.